ORIGINAL PAPER

Strength and Failure Mode of Expansive Slurry-Inclined Layered Rock Mass Composite Based on Mohr–Coulomb Criterion

Nan Yao[1,2] · Xingmin Deng[1,3] · Binyu Luo[1,2] · Felix Oppong[1] · Pengcheng Li[3]

Abstract

Traditional grouting technology only provides a bonding effect to surrounding rock fissures. Therefore, an expansion agent was added to the grouting material to provide compressive stress to the rock mass to make it more stable. Based on Mohr–Coulomb theory, the expression of the stress state of rock crack surface under different reinforcement methods and specimen strength under biaxial compression were derived. The action mechanism of grouting reinforcement on improving the strength of rock mass and the failure mode of rock mass after grouting are revealed. With the aid of the Digital Image Correlation (DIC) technique and ABAQUS software, the biaxial compression test and numerical simulation of expansive slurry-inclined layered rock mass composite (ESRC) with different contents of expansive agent were carried out, respectively. The results show that the strength of slurry-rock mass composite is higher with the expansive slurry grouting as compared with the regular slurry grouting. When the expansion agent contents are from 0 to 6%, the strength of the ESRC increased with an increase in the expansion agent content, the failure of ESRC occurred in the component with the lowest strength first. When there is little difference in strength between the weakest member and the sub-weak member, the failure occurred in these two components, while there is large difference in strength, the failure only occurred in the weakest component.

Highlights

- Through theoretical derivation, the strength expression of composite rock mass under different grouting conditions is obtained.
- The mechanism of grouting to improve the mechanical strength of rock mass is analyzed. And its failure mode is analyzed, which is of great significance to judge the strength and failure mode of composite rock mass.
- The theoretical analysis and numerical simulation results are consistent with the lab test results, and the lab test results show that expansive slurry can improve the strength of fractured rock mass better than regular slurry.

List of Symbols

$\theta, \varphi_\theta, c_\theta$	Crack dip angle, internal friction angle of crack surface, cohesion of crack surface, respectively
$\varphi_r, \varphi_s, \varphi_\theta^{rs}, \varphi_\theta^{es}$	Internal friction angle of rock mass, internal friction angle of slurry, internal friction angle of regular slurry, internal friction angle of expansive slurry, respectively
c_r, c_s, c^{rs}, c^{es}	Cohesion of rock mass, cohesion of slurry, cohesion of regular slurry, cohesion of expansive slurry, respectively

✉ Binyu Luo
luobinyu@wust.edu.cn

[1] School of Resources and Environmental Engineering, Wuhan University of Science and Technology, Wuhan 430081, China

[2] Hubei Key Laboratory for Efficient Utilization and Agglomeration of Metallurgic Mineral Resources, Wuhan 430081, China

[3] Sinosteel Maanshan General Institute of Mining Research Co., Ltd., Maanshan 243000, China

$\sigma_1, \sigma_3, \sigma_{ESRC}$	Maximum principal stress, minimum principal stress, strength of ESRC, respectively
$\sigma_\theta, \tau_\theta$	Normal stress on crack surface, shear stress on crack surface, respectively
$\sigma_\theta^{rs}, \tau_\theta^{rs}$	Normal stress and shear stress of crack surface after regular slurry grouting, respectively
$\sigma_e, \Delta f, \mu$	Expansion stress, friction increment, friction coefficient of crack surface, respectively
$\sigma_1^{rs}, \sigma_1^{es}$	Strength of crack surface after regular slurry grouting, strength of crack surface after expansive slurry grouting, respectively
$\sigma_1^\theta, \sigma_1^r, \sigma_1^s$	Strength of crack surface, rock mass, and slurry was expressed by maximum principal stress and minimum principal stress, respectively
$\sigma_c^\theta, \tau_c^r, \sigma_c^s$	Uniaxial compressive strength of crack surface, rock mass, and slurry, respectively
μ_θ, μ_r, μ_s	Minimum principal stress coefficient of crack surface, rock mass, and slurry, respectively

1 Introduction

In underground rock mass engineering, steeply inclined layered rock masses are often encountered in roadways construction (Zhou et al. 2019; Li et al. 2022), especially in complex geological strata composed of interlayered rocks and bedding planes that has transverse isotropy characters. Due to the poor mechanical properties of bedding planes, the strength and stiffness of transverse isotropic plane differs from those that are perpendicular in direction (Xu et al. 2017), resulting in the instability of steeply layered rock mass that causes a great challenge to the underground engineering construction. Therefore, the key to the effective support method in steeply inclined layered rock mass is the reinforcement and improvement of bedding planes.

At present, grouting reinforcement technology is widely used in the geotechnical engineering in steeply inclined rock mass (Saeidia et al. 2013; Wang et al. 2019; Lee et al. 2020). Grouting the bedding planes increases the friction and cohesive force; thus, the weak interlayered rock is bonded as a whole, and the overall stability of the rock mass is improved (Gothäll and Stille 2009, 2010; Celik and Akcuru 2020). The Portland cement is a traditional grouting material that provides only bonding force to the joint rock mass but not squeezing effect (unless grouting with high pressure).

Furthermore, Portland cement undergoes dry shrinkage after solidification, that may affect bonding performance (Panchmatia et al. 2020; Zhang et al. 2020; Zhang and Scherer 2020).

Basically, rock strength is greater in a three-dimensional stress state than in a one-dimensional stress state (Liu et al. 2020; Das and Singh 2020; Zhang et al. 2022). Therefore, adding an appropriate amount of expansion agent into the slurry will produce a certain volume expansion during the bonding process. The expansion agent squeezes and compacts the rock mass through its own volume expansion that changes the stress state of the supported rock mass, and improves the bearing capacity of the surrounding rock, resulting in the improvement of grouting reinforcement effect.

At present, many scholars have carried out grouting tests with different grouting materials to study the mechanical properties between slurry and rock mass after grouting reinforcement. García Calvo et al. (2020) prepared expansive slurry with ettringite and CaO as the raw materials, and characterized the expansion and mechanical properties of the slurry. Saeed et al. (2020) prepared expansive slurry with carbon fiber polymer as the filling material of anchor rod, and studied the bonding performance of filled anchor rod through pull-out test. Chen et al. (2021) studied the influence of geometry on the axial mechanical properties and failure mode of slurry by preparing cylindrical and cubic samples. The research showed that the strength of cubic samples was higher than that of cylindrical samples. Zhao and Zhou (2016) carried out experiment on rock samples with single and double crack under grouting. Using uniaxial compression test, the variation law of the mechanical properties of the samples was studied. It was found that grouting mainly plays the role of transmitting stress and reducing stress concentration at the separation tip and bridge area. Li et al. (2020) studied the mechanical properties of grouting materials using the shear test and numerical simulation. The results showed that the damage started from the weakest part of the material, and the improvement of the mechanical properties of grouting materials was useful to the reinforcement of rock cracks. In addition, based on the above research, many scholars further improved the grouting reinforcement effect by applying pre-stress in the grouting process, such as the bolt and grouting combined reinforcement method (Chen et al. 2014; Zou and Zhang 2021).

After grouting, the rock mass and slurry form a composite rock mass that influence the strength and failure modes by the individual action of the rock mass and the slurry. Predicting the accuracy of the strength and failure mode of the composite rock mass after grouting is a significant approach, that reveals the reinforcement mechanism of grouting. The Mohr–Coulomb criterion is widely used in the field of rock mechanics (Shen et al. 2018; Si et al. 2019; Lepakshi

and Venkatarama Reddy 2020) to predict the strength and failure mode of the composite rock mass. Many scholars have proven over the years its reliability and applicability through several studies. In the pre-test, the failure mode of ESRC material is mainly shear failure during the test, which complies with the failure characteristics described by Mohr–Coulomb criterion. Thus, the Mohr–Coulomb criterion is selected as the criterion of ESRC. Wu et al. (2019) estimated the horizontal stress of underground rock mass using the Mohr–Coulomb criterion based on the limit equilibrium condition, and verified the accuracy of the estimated model through the field test results. Luo et al. (2020) established the strength model of rock mass under the influence of compression shear characteristics and dip angle using the combination test results of compression shear and Mohr–Coulomb criterion, and revealed the mechanism of rock material weakening by dip angle effect. In addition, many scholars have studied the mechanical properties of composite rock mass under different reinforcement methods through theoretical derivation, laboratory test, and numerical simulation.

Based on the Mohr–Coulomb criterion, the grouting reinforcement mechanism, the strength and failure mode of ESRC after grouting are explored. Through laboratory test, the prefabricated single fractured rock samples are taken as the research objects. Cement and high-efficiency soundless crush agent are used as the raw materials to prepare the expansive slurry to reinforce the fractured rock masses (Yao et al. 2021a, b). The stress state of the samples is simulated by biaxial compression test; combining the DIC technology and numerical simulation, the strength, failure characteristics, and displacement variation of ESRC samples with different expansive agent contents are studied.
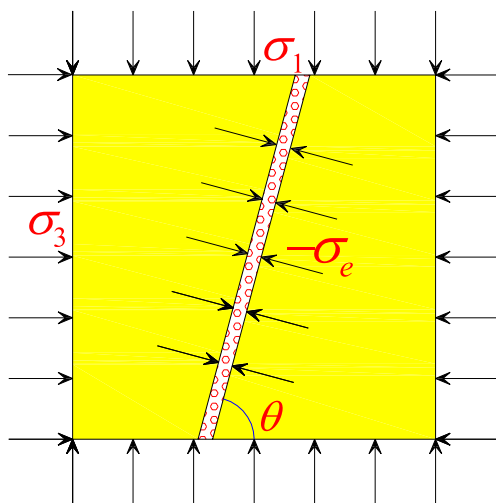

Fig. 1 Mechanical model of ESRC

2 Strength Criterion of ESRC

After injecting expansive slurry into the bedding plane of steeply inclined layered rock mass, the slurry will produce volume expansion on the bedding plane, and produce expansion stress that restrains the rock mass. The stress state of the rock mass will be improved under the joint action of the bonding force of the slurry and the constraint stress of surrounding rock.

The mechanical model of ESRC is shown in Fig. 1. The bedding plane element is regarded as a crack. The crack dip angle is θ, the cohesion of the crack surface is c_θ, and the internal friction angle is φ_θ. Assuming that the rock mass is constrained by the maximum principal stress (σ_1) and the minimum principal stress (σ_3), the stress along the crack depth remains unchanged; thus, the stress state can be considered as plane stress state. After injecting the expansive slurry, it will produce expansion stress (σ_e) to the bedding plane.

According to the Saint Venant's principle, when the expansion stress is less than the constraint stress of the surrounding rock mass, and the crack size is much smaller than the size of the composite rock mass itself, the expansion stress generated by the expansive slurry only acts near the crack surface, while the constraint stress state of the rock mass boundary is almost unchanged. As a result, basic assumptions made for the rock are as follows. Except for the bedding plane, the rock mass on both sides is isotropic and homogeneous.

The strength of the above model is determined by the minimum value of the crack surface and the rock mass strength. Under the action of the same minimum principal stress, when they reach the limit equilibrium state, the lower corresponding maximum principal stress will cause rock's failure first. According to the mechanical equilibrium conditions, the normal stress (σ_θ) and the shear stress (τ_θ) of the crack surface can be calculated as follows.

$$\sigma_\theta = \frac{1}{2}(\sigma_1 + \sigma_3) + \frac{1}{2}(\sigma_1 - \sigma_3)\cos 2\theta \tag{1}$$

$$\tau_\theta = \frac{1}{2}(\sigma_1 - \sigma_3)\sin 2\theta \tag{2}$$

Based on the Mohr–Coulomb criterion, the shear stress of the crack surface meets the following equation.

$$\tau_\theta = c_\theta + \sigma_\theta \tan \varphi_\theta \tag{3}$$

From Eqs. (1)–(3), the expression of the crack surface strength expressed by the maximum principal stress and the minimum principal stress under Mohr–Coulomb criterion can be obtained in the following equation.

a Without grouting   **b** Regular slurry   **c** Expansive slurry
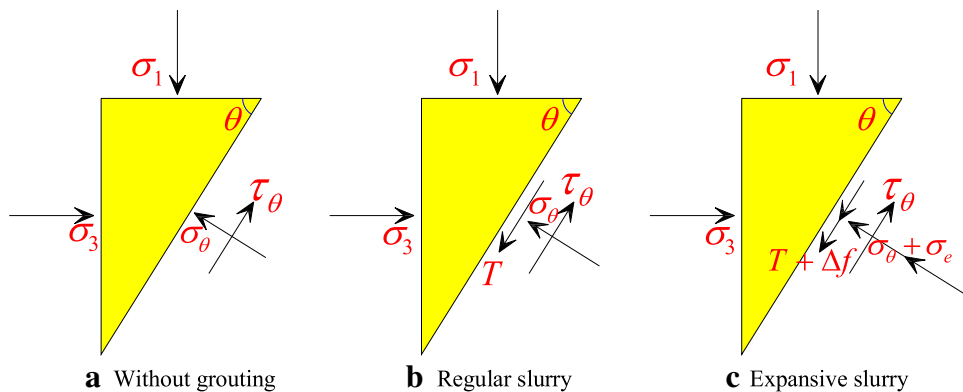
$$\sigma_1^\theta = \frac{2(c_\theta + \sigma_3 \tan \varphi_\theta \sin 2\theta)}{(1 - \tan \varphi_\theta \cot \theta) \sin 2\theta} \qquad (4)$$

The stress state of the rock mass crack surface is shown in Fig. 2. The three conditions expressed are without reinforcement, regular slurry and expansive slurry reinforcement, respectively.

Comparing the without grouting state (see Fig. 2(a)), with the regular slurry grouting, the bonding force (T) caused by the slurry condensation will be generated on the crack surface (shown Fig. 2(b)). The bonding force is the force generated by the rock mass after being reinforced. It is opposite to the direction of shear stress (τ_θ) under the action of principal stress. In addition, to the bonding force, the crack surface is also subject to the expansion stress (σ_e) and the increased friction (Δf) due to the increase of the normal force on the crack surface after the expansive slurry grouting (shown Fig. 2(c)). Therefore,

$$\Delta f = \mu \sigma_e \qquad (5)$$

The expressions of the normal stress (σ_θ^{rs}) and the shear stress (τ_θ^{rs}) on the crack surface under the reinforcement of regular slurry grouting are as follows, respectively.

$$\sigma_\theta^{rs} = \sigma_\theta = \frac{1}{2}(\sigma_1 + \sigma_3) + \frac{1}{2}(\sigma_1 - \sigma_3) \cos 2\theta \qquad (6)$$

$$\tau_\theta^{rs} = \frac{1}{2}(\sigma_1 - \sigma_3) \sin 2\theta - T \qquad (7)$$

Similarly, the shear stress of the crack surface based on the Mohr–Coulomb criterion satisfies

$$\tau_\theta^{rs} = c_\theta^{rs} + \sigma_\theta^{rs} \tan \varphi_\theta^{rs} \qquad (8)$$

From Eqs. (6)–(8), the expression of crack surface strength (σ_1^{es}) after regular slurry grouting reinforcement expressed by maximum principal stress and minimum principal stress based on Mohr–Coulomb criterion is as follows.

$$\sigma_1^{rs} = \frac{2(c_\theta^{rs} + \sigma_3 \tan \varphi_\theta^{rs} \sin 2\theta + T)}{(1 - \tan \varphi_\theta^{rs} \cot \theta) \sin 2\theta} \qquad (9)$$

Similarly, the expression of crack surface strength (σ_1^{es}) expressed by maximum principal stress and minimum principal stress after expansive slurry grouting reinforcement based on Mohr Coulomb criterion is as follows.

$$\sigma_1^{es} = \frac{2[c_\theta^{es} + (\sigma_3 \sin 2\theta + \sigma_e) \tan \varphi_\theta^{es} + T + \mu \sigma_e]}{(1 - \tan \varphi_\theta^{es} \cot \theta) \sin 2\theta} \qquad (10)$$

When the grouting crack has a certain width, the rock mass reinforced by grouting can be regarded as a composite rock mass sample with rock mass and slurry. When the rock masses have the same properties on both sides, the mechanical properties of the two sides of the slurry are the same. Therefore, only one side of the rock mass is considered.

Both the slurry and the rock mass comply with the Mohr–Coulomb criterion. The strength expressions of the rock mass (σ_1^r) and the slurry (σ_1^s) expressed by maximum principal stress and minimum principal stress are as follows.

$$\sigma_1^r = \frac{1 + \sin \varphi_r}{1 - \sin \varphi_r} \sigma_3^r + \frac{2c_r \cos \varphi_r}{1 - \sin \varphi_r} \qquad (11)$$

$$\sigma_1^s = \frac{1 + \sin \varphi_s}{1 - \sin \varphi_s} \sigma_3^s + \frac{2c_s \cos \varphi_s}{1 - \sin \varphi_s} \qquad (12)$$

where σ_3^r, σ_3^s are the confining stress of rock mass and slurry under compression. For expansive slurry, the confining stress is the sum of the initial confining stress and the expansion stress ($\sigma_3^{es} = \sigma_3^s = \sigma_3 + \sigma_e$).

According to the above analysis, the theoretical strength of the composite rock mass is determined as shown in Eq. (13).

$$\sigma_{ESRC} = \min(\sigma_1^\theta, \sigma_1^r, \sigma_1^s) \qquad (13)$$

From Eqs. (4), (9), (10), (11), (12), it can be found that when the rock mass and slurry parameters are determined,

the maximum principal stress (σ_1) of the crack surface is a function of the minimum principal stress (σ_3). Obviously, if the minimum principal stress is constant, the relationship between the three is $|\sigma_1^{es}| > |\sigma_1^{rs}| > |\sigma_1^{\theta}|$. After expansive slurry grouting, when the crack surface reaches the limit equilibrium state, the value of the corresponding maximum principal stress will increase as well as the overall strength.

3 Initial Failure Mode of ESRC

Obviously, the maximum principal stress (σ_1) of the rock mass and the slurry is also a function of the minimum principal stress (σ_3). When the minimum principal stress (σ_3) is equal to 0, the uniaxial compressive strength (UCS) of the crack surface, the rock mass, and the slurry are demonstrated by Eqs. (14)–(16), respectively.

$$\sigma_c^{\theta} = \sigma_1^{es} = \frac{2[c_{\theta}^{es} + (\sigma_3 \sin 2\theta + \sigma_e) \tan \varphi_{\theta}^{es} + T + \mu \sigma_e]}{(1 - \tan \varphi_{\theta}^{es} \cot \theta) \sin 2\theta} \quad (14)$$

$$\sigma_c^{r} = \frac{2c_r \cos \varphi_r}{1 - \sin \varphi_r} \quad (15)$$

$$\sigma_c^{s} = \frac{2c_s \cos \varphi_s}{1 - \sin \varphi_s} \quad (16)$$

$\sigma_c^{\theta}, \sigma_c^{r}, \sigma_c^{s}$ represent the uniaxial compressive strength of the crack surface, the rock mass, and the slurry, respectively.

According to the first-order function relationship between the maximum principal stress (σ_1) and the minimum principal stress (σ_3), the derivation of the minimum principal stress is obtained. The slope of the minimum principal stress of crack surface, rock mass, and slurry with respect to the maximum principal stress is also obtained.

$$\mu_{\theta} = \frac{d\sigma_1^{\theta}}{d\sigma_3} = \frac{2 \tan \varphi_{\theta}^{rs}}{(1 - \tan \varphi_{\theta}^{rs} \cot \theta)} \quad (17)$$

$$\mu_r = \frac{d\sigma_1^{r}}{d\sigma_3} = \frac{1 + \sin \varphi_r}{1 - \sin \varphi_r} \quad (18)$$

$$\mu_s = \frac{d\sigma_1^{s}}{d\sigma_3} = \frac{1 + \sin \varphi_s}{1 - \sin \varphi_s} \quad (19)$$

When Eqs. (18) and (19) are included $\varphi_r, \varphi_s \in (0, \frac{\pi}{2})$, μ_r and μ_s are always greater than 0. For steeply inclined layered rock mass, (if satisfied this statement is not clear) $\theta \in (\frac{\pi}{4}, \frac{\pi}{2})$; therefore, $\sin 2\theta$ is greater than 0 and $\cot \theta$ is less than 0. When $\varphi_{\theta}^{es} \in (0, \frac{\pi}{2})$, $\tan \varphi_{\theta}^{es}$ is also greater than 0, and μ_{θ} is always greater than 0. Then the minimum principal stress corresponding to the above three is an increasing function of the maximum principal stress.
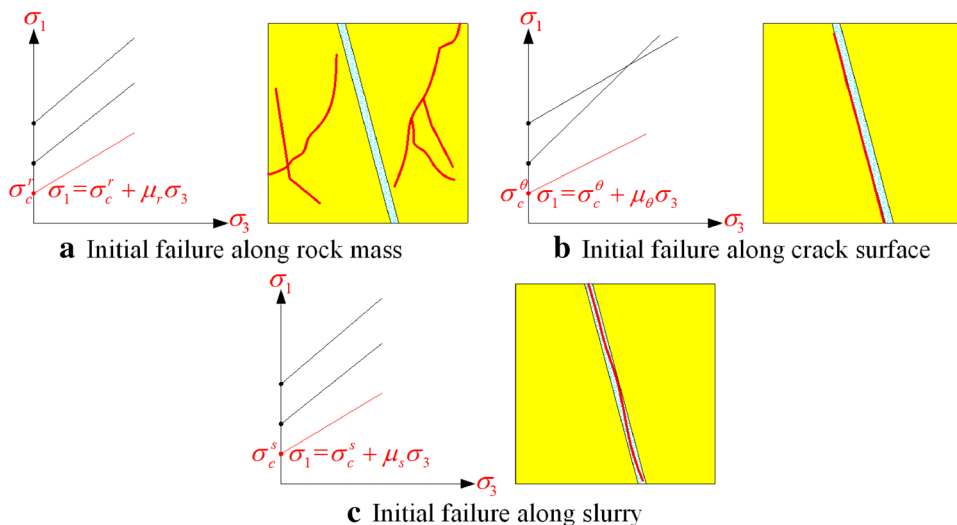
Assumed that the minimum principal stress remains unchanged during loading, and the mechanical properties between the two cementation surfaces are the same. According to the above analysis, the strength of the composite rock mass is related to the uniaxial compressive strength of its components and the slope of the minimum principal stress (σ_3) with respect to the maximum principal stress(σ_1).

The initial failure modes of ESRC are discussed as follows through the relationship between the components of Eqs. (14)–(19) corresponding to the uniaxial compressive strength and the slope.

Failure occurs first along a single component, specifically along the crack surface, in the rock mass, or the slurry.
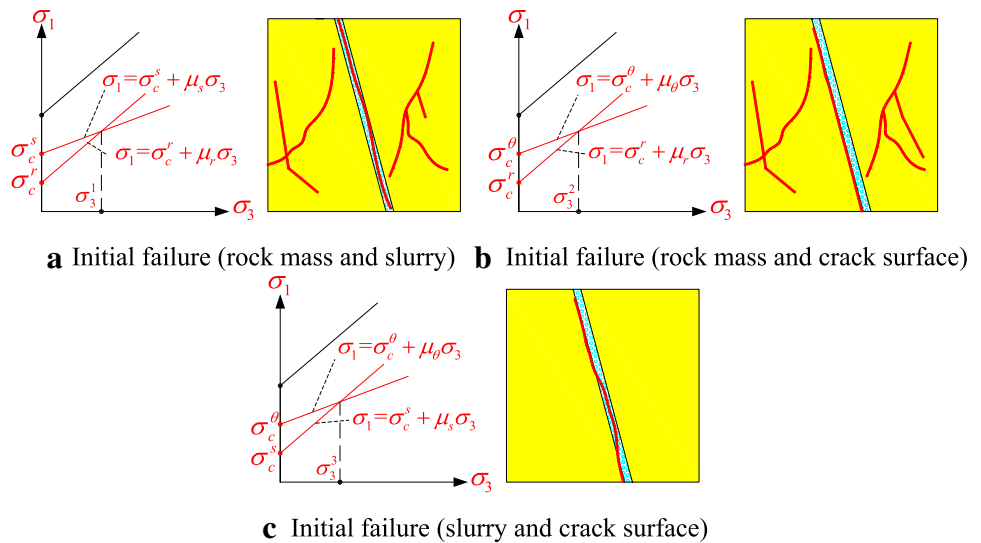
The failure occurs first along any two components; thus, simultaneous failure along the crack surface and rock mass, simultaneous failure along the crack surface and through slurry, or simultaneous failure along the rock mass and slurry.

Fig. 3 Strength relationship of rock mass under the first failure of single component

a Initial failure along rock mass

b Initial failure along crack surface

c Initial failure along slurry

Fig. 4 Simultaneous failure along two components

a Initial failure (rock mass and slurry)   **b** Initial failure (rock mass and crack surface)

c Initial failure (slurry and crack surface)

Failure occurs simultaneously along or in the three components.

The failure mode corresponding to Fig. 3 is that the failure occurs first along a single component. Taking Fig. 3(a) as an example, the uniaxial compressive strength of the rock mass will be the lowest of the three. Also, the slope of the corresponding minimum principal stress with respect to the maximum principal stress will be the lowest.

Figure 4 shows the simultaneous failure of ESRC along two components in the rock, the crack surface or the slurry. Taking Fig. 4(a) as an example, the uniaxial compression strength of the crack surface is the highest. Also, the corresponding slope (μ_θ) is the highest. At this time, the stress on both sides is $\sigma_3 = \sigma_3^r$, and the corresponding confining stress can be calculated by simultaneous Eqs. (11) and (12). When the stress on both sides is less than or greater than σ_3^r, the rock mass will fail along the component with the lowest strength. In the same way, the corresponding confining stress can also be calculated when the ESRC samples fail simultaneously along the rock interior and the crack surface, and along the slurry interior and crack surface.

Figure 5 shows that the ESRC sample fails simultaneously along the rock mass, on the crack surface, and in the slurry. In this situation, the corresponding confining stress

is calculated by the simultaneous Eqs. (4), (11), and (12). When the stress on both sides is less than or greater than σ_3^r, the ESRC will have a single component failure mode along the component with the lowest strength.

4 Biaxial Compression Test and Numerical Simulation

Based on the above theoretical derivations, the laboratory test and numerical simulation methods are applied to study the strength change law and failure characteristics of the samples under different grouting conditions. The specific test scheme is as follows.

4.1 Experiment Scheme of Lab Test

The raw materials for preparing the rock mass sample include cement and quartz sand. The materials for preparing the expansive slurry include cement, expansive agent, and accelerator. The crack inclination of the sample is 75° and the crack width is 6 mm. To realistically simulate the bedding surface, the crack contour is generated by random function, and the roughness is 1.14. The crack mold was made by 3D printing technology. The size of each square mold is $100 \times 100 \times 100$ mm. The expansive slurry with expansion agent content of 0%, 3%, 6%, and 9% was selected.

A membrane stress sensor was installed on the side wall of the mold before the slurry was poured to test the binding force of the samples under the action of grouting reinforcement. To ensure that the samples were always in a constrained state during the curing process, the experimental setup was not removed until the sample grouting was
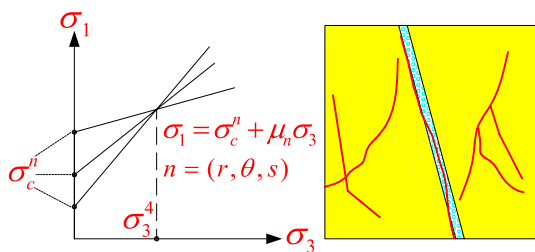
Fig. 5 Simultaneous failure along rock mass, fracture surface, and slurry

Table 1 Mechanical parameters of sample

Type	(UCS) /MPa	Cohesion /MPa	Internal friction angle /°
Rock mass	18.20	4.42	38.21
Regular slurry (0%)	23.64	5.84	37.24
Expansive slurry (3%)	21.59	5.46	34.13
Expansive slurry (6%)	18.97	5.07	29.91
Expansive slurry (9%)	12.14	3.71	24.80

complete for the loading test. The biaxial compression test was carried out after the specimen was cured.

In addition, according to the mechanical parameters of the rock mass and the slurry, the corresponding rock mass samples and slurry samples were prepared. The mechanical parameters of the rock mass and the slurry measured after curing are shown in Table 1.

4.2 Samples Preparation

(1) Mold preparation

First, the cleaned iron mold was fixed, a release agent was applied, and the 3D printed mold on the iron mold was installed to form a combined mold. The prefabricated crack spacer was inserted into the clamping slot of the mold and was weighed.

(2) Crack samples

The raw materials were prepared according to their proportions and was poured into the mold. It was then shaken on the shaking table for 30 s to ensure the flatness and the uniformity of the sample surface. The spacer was taken when the sample reached the initial setting state. The mold was then disassembled after 72 h. The samples were placed into a 20 °C constant temperature curing box for curing for 7d.
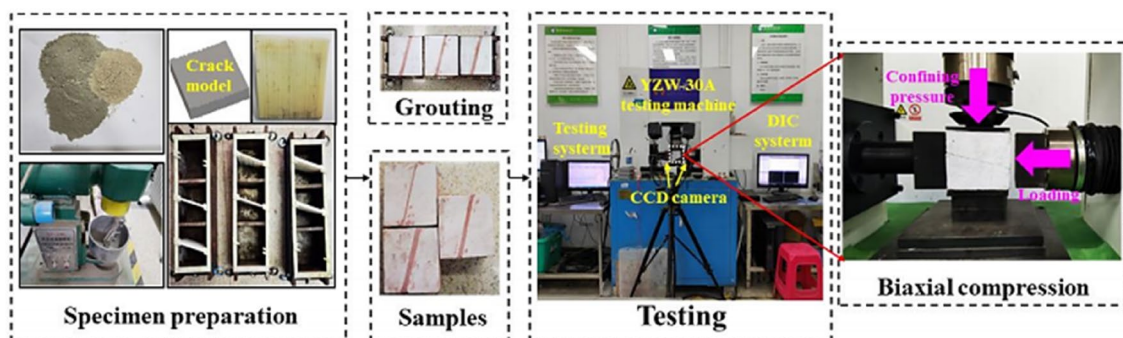
(3) Slurry injection

When the curing time of the samples was complete, the paired samples were placed back into the square model and it was ensured that the they were stuck to the side wall of the mold on the side opposite to the crack. The expansive slurry was then injected into the crack. Before the grouting, a thin-film stress sensor was installed on the side wall of the mold to test the expansion stress of the sample in the mold. To distinguish the slurry and the rock sample, a little red pigment that does not react with the slurry raw materials was mixed with the expansive slurry during preparation.
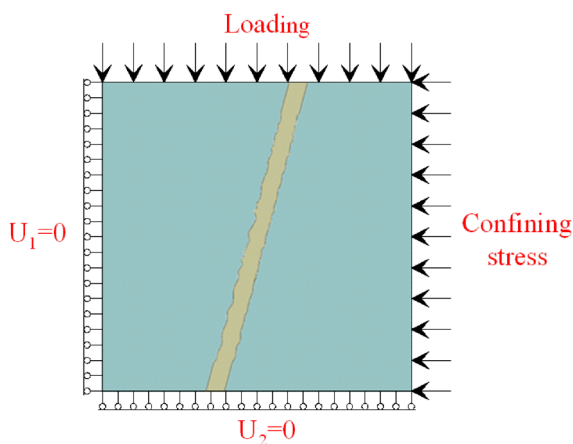
4.3 Biaxial Compression

When the grouting curing time was complete, the cured samples were prepared into speckle samples, and the displacement change characteristics of the samples during the loading failure process were monitored by DIC system. The loading system was YZW-30A microcomputer that is controlled by electronic rock direct shear instrument, and it has a load displacement control. The loading rate is 0.02 mm/min. A basic confining stress (1 MPa) was applied to all the samples. Also, an additional confining stress was added according to the expansion stress σ_e of each sample. When the confining stress of the sample was stable, the axial loading and the DIC system were started at the same time. The lab test process is shown in Fig. 6.

4.4 Numerical Simulation

The numerical simulation method is used as a comparison between theoretical and experimental methods. The ABAQUS software whose operation is based on the finite element method was used to conduct the numerical simulation. A size of 100×100 mm square dimension was used as the calculation model of the ESRC sample. The Mohr–Coulomb criterion and the plane strain (CPE4R) element were selected. A cohesive element was embedded at one of the two crack surfaces to define the tangential shear strength behavior and also simulate the bonding force of the slurry.

Fig. 6 Lab test process

Fig. 7 Numerical simulation model

Table 2 Expansion stress under different expansive agent content

Expansion agent content (%)	Expansion stress (MPa)
0	0
3	0.38
6	0.56
9	0.80

Table 3 Mechanical parameters of fractured rock sample and crack surface after grouting

Type	Shear strength / Mpa	Cohesion /Mpa	Internal friction angle /°
Fractured rock sample (no slurry)	2.14	–	22.12
Crack surface (0%)	5.52	4.56	32.61
Crack surface (3%)	5.61	4.65	37.43
Crack surface (6%)	5.73	4.83	39.94
Crack surface (9%)	5.53	3.84	35.75

When the shear stress reaches the shear strength, the element will break and fail.

The boundary condition was consistent with the biaxial compression test. The horizontal displacement (U_1) of the left boundary and the vertical displacement (U_2) of the bottom boundary were limited. The constraint stress that was consistent with the test was applied on the right side, and the linear displacement loading was applied on the upper side. The material parameters of the model are shown below. The numerical model is shown in Fig. 7.

5 Test Results

5.1 Strength Characteristics

Some ESRC samples were prepared to test the expansion stress and the mechanical parameters of the crack surface after grouting. The expansion stress of the samples with different expansive agent contents is shown in Table 2.

To test their shear strength, the cohesion and the internal friction angle with the different expansive agent contents, the shear test was carried out on the fractured rock sample and the grouted sample to test the mechanical parameters of the samples. The σ_e is also concerned in the shear test which is added to the confining stress, as shown in Table 3.

According to the difference between the shear strength of the fractured rock sample and the grouted sample, the bonding force (T) value generated by the slurry was 3.38 MPa. Assuming that the bonding force of the regular slurry and the expansive slurry was the same, the friction coefficient of crack surface is equal to 0.34 calculated by Eq. (10).

The mechanical parameters of the rock mass, the slurry, and the crack surface in Tables 1 and 3 are substituted into Eqs. (10)–(13) for calculation. The results obtained by theoretical calculation, experiment and numerical simulation are shown in Fig. 8.

As shown in Fig. 8, the minimum strength of the three components is the theoretical strength of the sample. When the expansive agent was 0–6%, the strength of the sample increased with the increase in the expansive agent content. When the expansion agent was 9%, the strength of the sample decreased obviously, because of the strength decrease of expansive slurry with higher expansion agent. It shows that when the expansive agent increased to a certain value, the strength of the slurry was low, resulting in the reduction of the overall strength of the rock mass.

When the expansion agent was 0%, 3%, 6%, and 9%, the relative errors between the theoretical calculation strength and the lab test strength of the ESRC samples were 5.70%, 4.81%, 9.40%, and 17.83%, respectively. Also, the relative errors between the numerical simulation strength and the lab test strength were 4.50%, 2.77%, 11.34%, and 9.33%. Because of the weak strength of the slurry itself, the samples with 9% expansion agent content recorded the highest error among the others. The theoretical calculation, the lab test, and the numerical simulation strength are well in agreement with each other, which shows the correctness and effectiveness of this research.

Figure 9 shows the axial stress contour when the model failed. When the expansive agent was 0%, 3%, 6%, 9%, the maximum stress was distributed at the crack surface, the crack surface, the slurry and rock mass, and the slurry, respectively. It can be seen from Fig. 8 that when the expansion agent was 6%, the test strength of the ESRC sample
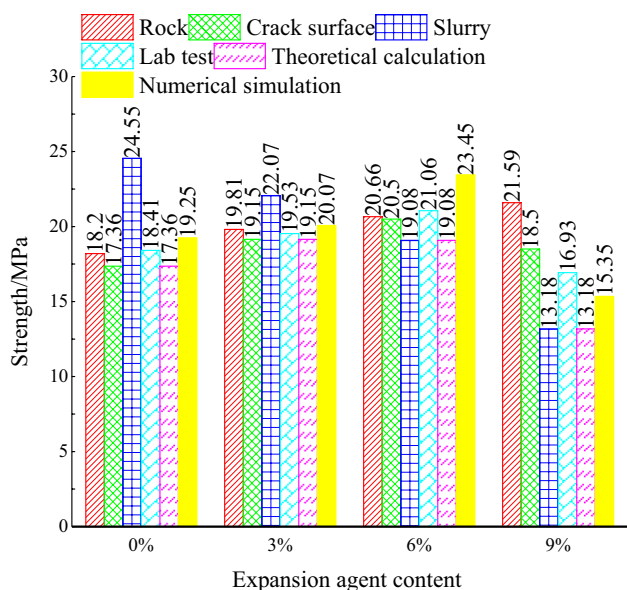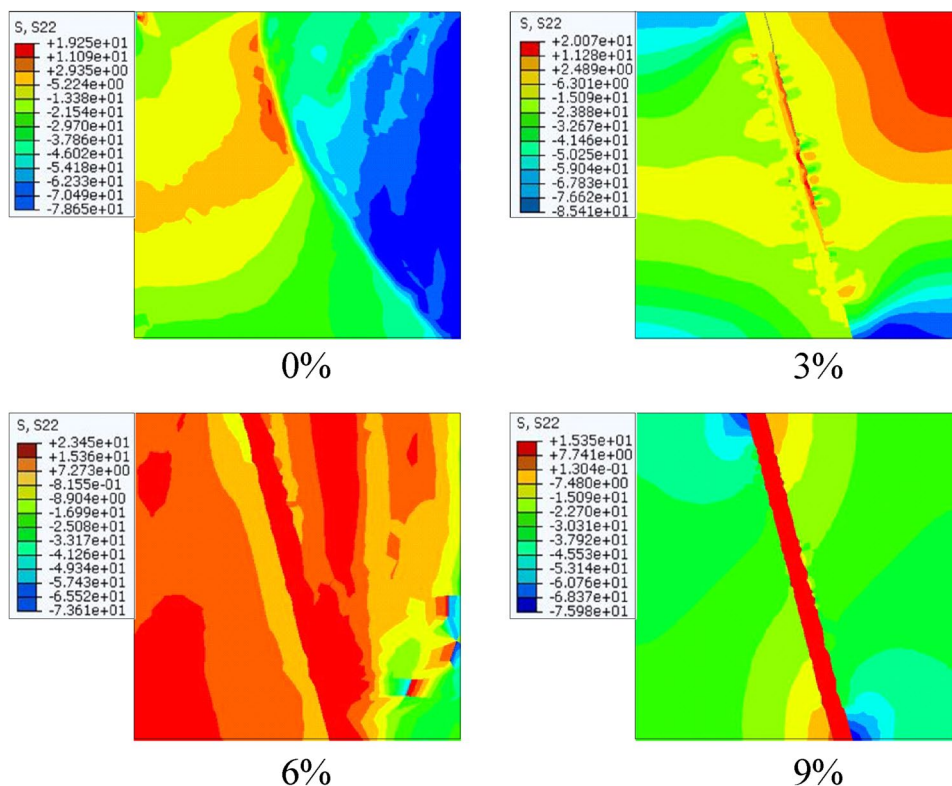
Fig. 8 Theoretical strength, test strength, and calculation strength

was greater than the other three components. This shows that an appropriate expansion stress of the expansion slurry can improve the strength of the fractured rock mass. This is consistent with the results of the maximum stress distribution of the slurry and the rock mass when the sample failed in the numerical model.

5.2 Analysis of Typical Stress–Strain Curves

The typical stress–strain curves of the ESRC samples with the expansion agent contents of 0%, 3%, 6%, 9% are shown in Fig. 10.

From Fig. 10, the compaction phase, the elastic deformation phase, the plastic yield phase, and the post-peak failure phase of the ESRC samples are different, due to the differences of the expansive agent contents.

When the expansive agent was low, the linear elasticity phenomenon was not clear. It was relatively gentle after loading to a certain extent, and then started increasing. For the samples with high expansive agent, a clear linear elasticity was seen and lasted for a longer period of time.

When the expansive agent contents were 3% and 6%, there were multiple peaks in the yield phase. Also, when the expansion agents were 0% and 9%, the yield phase of the samples was relatively gentle.

When the expansive agent contents were 3% and 6%, the strength of the samples decreased rapidly after reaching the peak strength, and the brittleness characteristics were clear, but the bearing capacity was weak. When the expansive agent contents were 0% and 9%, the strength decreased slowly after reaching the peak strength, and the post-peak-bearing capacity was stronger.

When the expansion agent content was 0%, the ductility characteristics were clear after reaching the peak strength. When the expansion agent contents were 3% and 6%, due to the effect of the expansion stress, the internal compactness
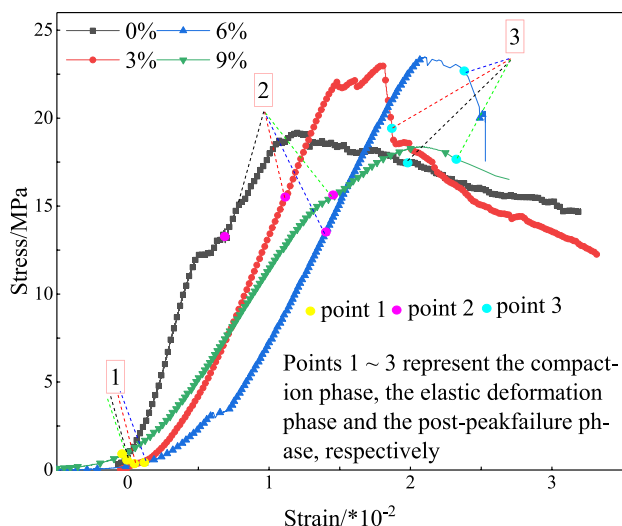
Fig. 9 The axial stress contour of models under different expansion contents

Fig. 10 Typical stress–strain curve

of the sample was better than the regular slurry, showing a clear brittleness characteristic. When the expansive agent was 9%, the bearing capacity and compactness of the slurry were weaker than lowering the expansion agent contents and the samples showed ductility characteristics after reaching the peak strength.

To sum it up, the strength of the ESRC samples is 6% > 3% > 0% > 9%. Although the slurry with 9% expansion agent content has the highest expansion stress, but the overall strength of the ESRC sample is the lowest. It shows that the expansive slurry with higher expansive agent content may generate higher expansion stress but has weaker strength of itself, which may be unbeneficial for the strength improvement of ESRC samples.

5.3 Failure Mode

The failure characteristics of the ESRC samples differ with different expansion agent contents. According to the strength of the ESRC samples and initial failure mode, the weakest component determines the initial failure section. Different expansion agent contents in the crack rock mass causes different expansion pressure, that leads to the differences in the strength of rock, the slurry, and the crack surface. The strength of each component and the determination of the initial failure component are calculated according to Eqs. (10)–(13), as shown in Table 4.

To further reveal the details of the deformation evolution during loading, the axial displacement and the final failure mode under different deformation states were observed. In ABAQUS, equivalent plastic strain (PEEQ) is a cumulative value that describes the increase in plastic deformation of a material. When PEEQ is greater than 0, it indicates that the material has failed. The results are shown in Fig. 11.

In the middle and the late stage of the elastic deformation phase (point 2, Fig. 11), the component with the lowest strength produced more displacement first, which was quite different from the surrounding components. The cracks appeared first at these places during the continuous loading. As shown in Fig. 11, the expansion agent contents were 0% and 3%, the samples first produced more displacement at the crack surface. When the expansion agent contents were 6% and 9%, the samples produced more displacement in the slurry first. When a large displacement occurs at a component, it indicates that there is a tendency of failure, and this is completely consistent with the theoretical calculation results.

The test strength was greater than the theoretical strength. The reason is that, after the weakest component was damaged, the crack at the component was tightly closed by the confining pressure on both sides. When the bearing capacity of the other components is strong, the samples also will

Table 4 Determination of failure mode

Expansion agent (%)	Components	Theoretical calculation strength /MPa	Lab test strength /MPa	Initial failure component
0	Rock	18.20	18.41	Crack surface
	Crack surface	17.36		
	Slurry	24.55		
3	Rock	19.81	19.53	Crack surface
	Crack surface	19.15		
	Slurry	22.07		
6	Rock	20.66	21.06	Slurry
	Crack surface	20.50		
	Slurry	19.08		
9	Rock	21.59	16.93	Slurry
	Crack surface	18.50		
	Slurry	13.18		
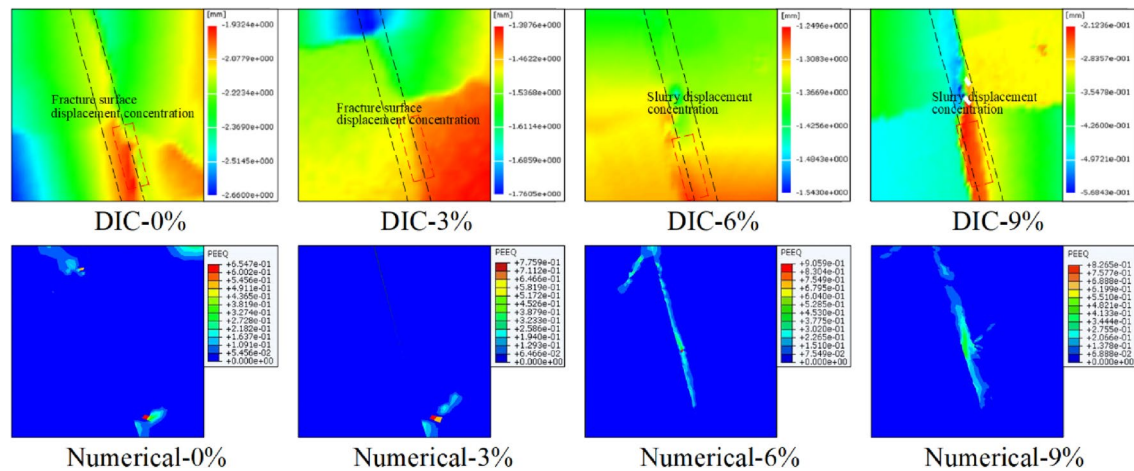
Fig. 11 Initial failure component and PEEQ (point 2)

have a certain bearing capacity. When the strength difference between the weakest component and other components is too high, the component will damage severely, and the samples will damage directly along the component.

The results show that the strength relationship of the rock mass, the slurry, and the crack surface is the main factor affecting the deformation and failure of the ESRC. The strength of the rock mass and the slurry determined the bearing capacity of the two parts of the ESRC. Due to the differences in the expansive agents, the compactness of the rock mass and the shear strength of the crack surface were also different. When the expansive agent content was low, the failure mode was mainly affected by the crack surface and the rock mass. With the increase in the expansive agent content, the failure mode was mainly affected by the slurry.

The axial displacement under different phases final failure mode of ESRC samples can be seen in Fig. 12

In Fig. 12 0%–1, 0%–2, and 0%–3 represent the compaction phase, elastic deformation phase, and post-peak failure phase of the samples with 0% expansion agent content, respectively. The state in the stress–strain curve is shown in points 1–3 in Fig. 10. It can be seen in Fig. 12 that the samples with 3% and 6% expansive agent contents exhibited more displacement at the boundary at the early stage of the compaction phase. The crack surface was affected by the expansion stress, and the internal compactness was slightly better than those at the boundary. In the compaction phase, after more displacement occurred at the boundary, the confining force decreased, and the loading device compensated it to the set value. When the sample boundary was pressed again, more displacement occurred.

In the middle and late stage of the elastic deformation phase, when the expansive agent contents were 0% and

3%, the maximum displacement of the sample appeared at the crack surface. When the expansion agent contents were 6% and 9%, the maximum displacement appeared at the slurry. This is completely consistent with the judgment made in Table 4.

When the expansive agent contents were 0% and 3%, the samples finally failed along the crack surface and the rock mass, and the rock mass failed severely. After the crack surface was damaged, the crack surface and the rock mass were continuously closed on both sides under the action of pressure to form a support. The failure of the rock mass with the weakest strength led to the general instability of the samples. When the expansion agent contents were 6% and 9%, the samples failed along the slurry and the rock mass. Due to the weak strength of the slurry, with the progress of loading, the slurry completely penetrates while the rock is still relatively complete. The damage of the sample is caused by the slurry.

When the expansive agent contents were 0% and 3%, the PEEQ was concentrated in the rock mass, and when the expansive agent contents were 6% and 9%, the PEEQ was mainly concentrated in the slurry. This is consistent with the experiment results.

The above result shows that when the samples reached the middle and late stage of the elastic deformation phase under biaxial compression, the component with the weakest strength produced more displacement and began to deform first. The crack at the weakest component was tightly closed by the confining pressure on both sides, and the sample continued to be loaded. During the loading progress, the component with the weaker strength continued to deform and produced more displacement. When the strength difference between the weakest and weaker components was low (crack surface (0%) and rock mass (3%)), the samples eventually failed along the two
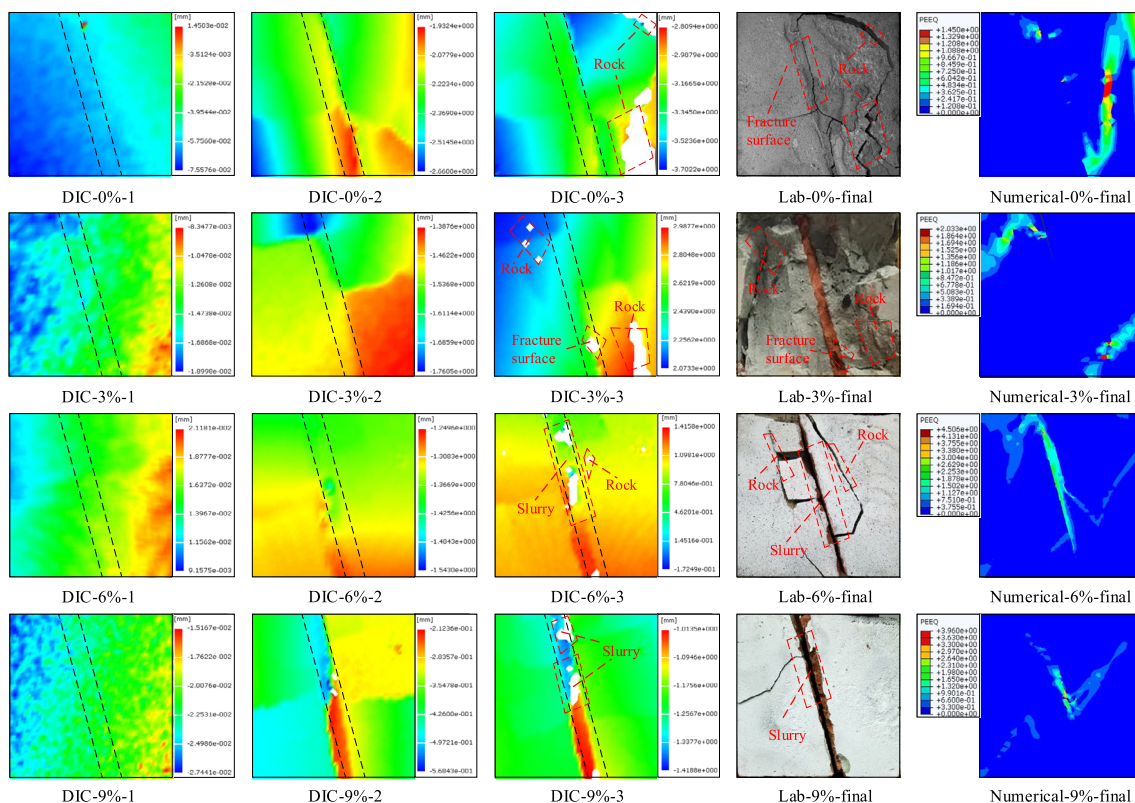
Fig. 12 Axial displacement under different phases and the final failure form

components. When the strength difference between the weakest and the other components was high, the component damaged severely, leading to the general instability failure of the sample.

Figure 12 shows that the failure mode of the ESRC samples from the lab test and the numerical simulation are also well in agreement with each other.

6 Conclusion

The theoretical analysis, the biaxial compression lab test, and numerical simulation were carried out for the expansive slurry grouted rock samples under different expansion stress. Based on the Mohr–Coulomb criterion, the stress expressions of rock mass without grouting, regular slurry grouting, and expansive slurry grouting were deduced in limit equilibrium state. The conclusions have been summarized as following.

(1) Expansive slurry grouting reinforcement can improve the compressive strength of the fractured rock mass. Compared with regular slurry, when the expansive agent contents were 3% and 6%, the strength of the ESRC samples increased by 6.08% and 12.58%, respec-

tively. The reinforcement mechanism is that the stress state of the slurry—rock bond surface changes because of the confining stress produced by expansive agent, and the maximum principal stress of the rock mass that reached the limit equilibrium state is higher than that of the rock mass without grouting and regular slurry.

(2) The failure condition of the samples indicates that the weakest component failed first. When the strength difference between the weakest and the second weakest component was low, the final failure may occur in these two components. When the weakest component was lower than the other components, the specimen eventually failed directly along the weakest component. The theoretical calculation strength and failure mode of ESRC samples were well in agreement with the lab test and numerical simulation results of those.

(3) With the increase of the content of expansion agent, the expansion stress increases, which was favorable to improve the strength of the crack surface, but its strength was relatively low reducing the overall strength of the composite sample. To ensure that the expansive slurry produces great expansion stress with well strength, it is necessary to carry out relevant research on improving the strength of the slurry with high expansive agent content. In addition, the strength

of the rock mass was close to the slurry, the grouting reinforcement effect to the slurry and rock with high strength difference will be carried out in the future study.

Data availability All data generated or analyzed during this study are included in this article.

Declarations

Conflict of Interest The authors declare that they have no known competing financial interests or personal relationships that could have appeared to influence the work reported in this paper.

References

Celik F, Akcuru O (2020) Rheological and workability effects of bottom ash usage as a mineral additive on the cement based permeation grouting method. Constr Build Mater 263:120186. https://doi.org/10.1016/j.conbuildmat.2020.120186

Chen C, Ting R, Cook C (2014) Introducing aggregate into grouting material and its influence on load transfer of the rock bolting system. Int J Rock Mech Min Sci 24(3):325–328. https://doi.org/10.1016/j.ijmst.2014.03.006

Chen JH, Hagan PC, Saydam S (2021) An experimental study of the specimen geometry effect on the axial performance of cement-based grouts. Constr Build Mater 310:125167. https://doi.org/10.1016/j.conbuildmat.2021.125167

Das R, Singh TN (2020) Effect of rock bolt support mechanism on tunnel deformation in jointed rockmass: a numerical approach. Undergr Space 6:409–420. https://doi.org/10.1016/j.undsp.2020.06.001

García Calvo JL, Pedrosa F, Carballosa P, Revuelta D (2020) Evaluation of the sealing effectiveness of expansive cement grouts through a novel water penetration test. Constr Build Mater 251:118974. https://doi.org/10.1016/j.conbuildmat.2020.118974

Gothäll R, Stille H (2009) Fracture dilation during grouting. Tunn Undergr Space Technol 24(2):126–135. https://doi.org/10.1016/j.tust.2008.05.004

Gothäll R, Stille H (2010) Fracture–fracture interaction during grouting. Tunn Undergr Space Technol 25(3):199–204. https://doi.org/10.1016/j.tust.2009.11.003

Lee JS, Sagong M, Park J, Choi IY (2020) Experimental analysis of penetration grouting in umbrella arch method for tunnel reinforcement. Int J Rock Mech Min Sci 13:104346. https://doi.org/10.1016/j.ijrmms.2020.104346

Lepakshi R, Venkatarama Reddy BV (2020) Shear strength parameters and Mohr-Coulomb failure envelopes for cement stabilised rammed earth. Constr Build Mater 249:118708. https://doi.org/10.1016/j.conbuildmat.2020.118708

Li Z, Liu HX, Dun ZL, Ren LW, Fang JJ (2020) Grouting effect on rock fracture using shear and seepage assessment. Constr Build Mater 242:118131. https://doi.org/10.1016/j.conbuildmat.2020.118131

Li A, Liu Y, Dai F, Liu K, Wang K (2022) Deformation mechanisms of sidewall in layered rock strata dipping steeply against the inner space of large underground powerhouse cavern. Tunn Undergr Space Technol 120:104305. https://doi.org/10.1016/j.tust.2021.104305

Liu SW, He DY, Fu MX (2020) Experimental investigation of surrounding-rock anchoring synergistic component for bolt support in

tunnels. Tunn Undergr Space Technol 104:103531. https://doi.org/10.1016/j.tust.2020.103531

Luo BY, Ye YC, Hu NY, Wang WQ (2020) Investigation of dip effect on uniaxial compressive strength of inclined rock sample by experimental and theoretical models. Rock Mech Rock Eng 53:5659–5675. https://doi.org/10.1007/s00603-020-02234-9

Panchmatia P, Olvera R, Genedy M, Juenger M, van Oort E (2020) Shrinkage behavior of Portland and geopolymer cements at elevated temperature and pressure. J Petrol Sci Eng 195:107884. https://doi.org/10.1016/j.petrol.2020.107884

Saeed YM, Al-Obaidi SM, Al-hasany EG, Rad FN (2020) Evaluation of a new bond-type anchorage system with expansive grout for a single FRP rod. Constr Build Mater 261:120004. https://doi.org/10.1016/j.conbuildmat.2020.120004

Saeidia O, Stille H, Toribi SR (2013) Numerical and analytical analyses of the effects of different joint and grout properties on the rock mass groutability. Tunn Undergr Space Technol 38:11–25. https://doi.org/10.1016/j.tust.2013.05.005

Shen BT, Shi JY, Barton N (2018) An approximate nonlinear modified Mohr–Coulomb shear strength criterion with critical state for intact rocks. J Rock Mech Geotech Eng 10(4):645–652. https://doi.org/10.1016/j.jrmge.2018.04.002

Si XF, Gong FQ, Li XB, Wang SY, Luo S (2019) Dynamic Mohr–Coulomb and Hoek–Brown strength criteria of sandstone at high strain rates. Int J Rock Mech Min Sci 115:48–59. https://doi.org/10.1016/j.ijrmms.2018.12.013

Wang Q, Qin Q, Jiang B, Yu HC, Pan R, Li SC (2019) Study and engineering application on the bolt-grouting reinforcement effect in underground engineering with fractured surrounding rock. Tunn Undergr Space Technol 84:237–247. https://doi.org/10.1016/j.tust.2018.11.028

Wu F, Chen B, Zou QL, Zhao C, Liu W, Chen J, Ni GH (2019) Range estimation of horizontal stress of deep rock based on Mohr–Coulomb criterion. Results in Phys 12:2107–2111. https://doi.org/10.1016/j.rinp.2019.02.061

Xu DP, Feng XT, Chen DF, Zhang CQ, Fan QX (2017) Constitutive representation and damage degree index for the layered rock mass excavation response in underground openings. Tunn Undergr Space Technol 64:133–145. https://doi.org/10.1016/j.tust.2017.01.016

Yao N, Chen JW, Hu NY, Ye YC, Xiao YH, Huang Y (2021a) Experimental study on expansion mechanism and characteristics of expansive grout. Constr Build Mater 268:121574. https://doi.org/10.1016/j.conbuildmat.2020.121574

Yao N, Deng XM, Wang QH, Ye YC, Zhang WH, Liu YD (2021b) Experimental investigation of expansion behavior and uniaxial compression mechanical properties of expansive grout under different constraint condition. B Eng Geol Environ 80:5609–5621. https://doi.org/10.1007/s10064-021-02190-w

Zhang ZD, Scherer GW (2020) Measuring chemical shrinkage of ordinary Portland cement pastes with high water-to-cement ratios by adding cellulose nanofibrils. Cem Concr Compos 111:103625. https://doi.org/10.1016/j.cemconcomp.2020.103625

Zhang YG, Li LF, Xi YP, Hubler MJ (2020) Experimental and theoretical study of the restrained shrinkage cracking of early age well cement. Constr Build Mater 262:120368. https://doi.org/10.1016/j.conbuildmat.2020.120368

Zhang JP, Liu LM, Liu CX, Li Y (2022) Mechanism and application of new prestressed yield bolt for controlling deep high-stress rock mass. Tunn Undergr Space Technol. 119:104254. https://doi.org/10.1016/j.tust.2021.104254

Zhao ZH, Zhou D (2016) Mechanical properties and failure modes of rock samples with grout-infilledflaws: a particle mechanics modeling. J Nat Gas Sci Eng 34:702–715. https://doi.org/10.1016/j.jngse.2016.07.022

Zhou YY, Xu DP, Gu GK, Liu K, Wan LP, Wang TL, Yang JB (2019) The failure mechanism and construction practice of large underground

caverns in steeply dipping layered rock masses. Eng Geol 250:45–64. https://doi.org/10.1016/j.enggeo.2019.01.006

Zou JF, Zhang PH (2021) A semi-analytical model of fully grouted bolts in jointed rock masses. Appl Math Model 98:266–286. https://doi.org/10.1016/j.apm.2021.05.012

Publisher's Note Springer Nature remains neutral with regard to jurisdictional claims in published maps and institutional affiliations.